



## Stress behaviours of viscoelastic flow around square cylinder

Guler Bengusu TEZEL<sup>1\*</sup>, Kerim YAPICI<sup>2</sup>, Yusuf ULUDAG<sup>3</sup>

on the last page

<sup>1</sup>Department of Chemical Engineering, Faculty of Engineering and Architecture, Abant Izzet Baysal University, 14280, Bolu, Turkey<sup>2</sup>Department of Chemical Engineering, Faculty of Engineering and Architecture, Suleyman Demirel University, 32260, Isparta, Turkey<sup>3</sup>Department of Chemical Engineering, Middle East Technical University, 06800 Ankara, Turkey

Received: 8 April 2019; Revised: 20 May 2019; Accepted: 21 May 2019

\*Corresponding author e-mail: [gulerbengusutezel@ibu.edu.tr](mailto:gulerbengusutezel@ibu.edu.tr)

<b>Citation:</b> Tezel, G.B.; Yapici, K.; Uludag, Y. <i>Int. J. Chem. Technol.</i> 2019, 3 (1), 61-66.
--

## ABSTRACT

In this study, it is aimed the numerically investigation of the flow of liner PTT (Phan-Thien-Tanner) fluid, which is a viscoelastic fluid model over limited square obstacle by finite volume method. The finite volume method has been used for simultaneous solution of continuity, momentum and fluid model equations with appropriate boundary conditions. The effects of the inertia in terms of Reynolds number,  $Re$ , ( $0 < Re < 20$ ) and the of elasticity in terms of Weissenberg number,  $We$ , ( $1 < We < 15$ ) of PTT flow on vertical and shear stress areas are examined in detail.

**Keywords:** Square cylinder, confined channel, viscoelastic flow, PTT fluid.

## Kare silindir etrafındaki viskoelastik akışın stres davranışları

## ÖZ

Bu çalışmada viskoelastik akışkan modeli olan liner PTT (Phan-Thien-Tanner) akışkanın sınırlandırılmış kare engel üzerinden olan akışın sonlu hacimler yöntemi ile nümerik olarak incelenmesi hedeflenmiştir. Sonlu hacimler yöntemi, uygun sınır koşulları ile birlikte, süreklilik, momentum ve akışkan model eşitliklerinin eş zamanlı çözümü için kullanılmıştır. PTT akışın Reynolds sayısı,  $Re$ , ( $0 < Re < 20$ ) cinsinden eylemsizliğinin ve Weissenberg sayısı,  $We$ , ( $1 < We < 15$ ) cinsinden elastiğitesinin, dikey ve kayma gerilim alanları üzerine olan etkileri detaylı bir şekilde incelenmiştir

**Anahtar Kelimeler:** Kare silindir, sınırlandırılmış kanal, viskoelastik akış, PTT akışkan.

## 1. INTRODUCTION

Flow of fluids over the square obstacles is present in many engineering processes such as fins in heat exchangers, coating processes, cooling towers, extruders and membrane processes.<sup>1</sup> With such crucial industrial implications, hydrodynamics of such flows has been subject of many computational studies in the literature. There are many studies on Newtonian fluid flow around a circular obstacle. For instance, Hassanzadeh and co-workers.<sup>2</sup> performed numerical study on the flow around a sphere using finite volume method. They presented flow structures around sphere in terms of velocity,

streamlines, pressure distributions at high  $Re$  (Reynolds number) numbers. Their numerical predictions were also confirmed by the experimental visualizations. As an experimental visualization method, particle image velocimetry was used in this study. Particle Image Velocimetry (PIV) is used to carry out flow field measurements experimentally. This technique enables the qualitative and quantitative flow visualization of the flow field 2. Pioneer study on this geometry was given by Breuer and co-workers.<sup>3</sup> They analyzed laminar two-dimensional Newtonian flow around a square cylinder using finite volume and lattice Boltzmann methods.

In this study, blockage ratio  $B$ , is the ratio over the

obstacle dimension and channel height, was 1/8. The results obtained from two methods were also good agreement. They observed bigger wake size with increased  $Re$ . In the analysis by Sen and co-workers,<sup>4</sup> with  $B = 1/100$  Newtonian flow over a square obstacle for  $Re \leq 40$  was studied using a finite element formulation. They also modelled the flows over the cylinders of circular and elliptical ones. They reported effect of  $Re$  on the flow structure. In their recent study Puig-Aranega and co-workers<sup>5</sup> searched Newtonian flow around a square cylinder obstacle using lattice Boltzmann method for  $50 \leq Re \leq 100$ . They reported strong impact of imposed boundary conditions on the stress field around the cylinder. However, in the literature studies on non-Newtonian flow (inelastic flow) case over the obstacles are smaller than those Newtonian flows. Dhiman and co-workers<sup>6</sup> employed power-law fluids flow around a confined square cylinder using finite volume method. Other study of Dhiman and co-workers<sup>7</sup> showed stronger impact of power law fluids at low values of  $Re$  compared as to the high values of  $Re$ . Ehsan and co-workers<sup>8</sup> also studied the inertia effects on the flow fields under both laminar and turbulent conditions. Their main finding was that decreasing drag effects was observed when the inertial effects increased. Moreover, Nilmarkar and co-workers<sup>9</sup> obtained numerically Bingham plastic fluid flow past a square cylinder at  $Re = 0$ . The effect of Bingham number,  $B_i$  considered as a yielding stress parameter, on the stress and pressure fields was reported in their study. They observed the weaker dependence of flow fields on  $B_i$  at its increased values.

On the other hand, viscoelastic flow hydrodynamics are also significant for the industrial implications due to revealing both viscous and elastic effects on the flow field. Hence, this study mainly deals with the flow of a viscoelastic linear PTT (Phan-Thien-Tanner) fluid, around a confined square obstacle numerically.

## 2. NUMERICAL METHODOLOGY

Two-dimensional flow of linear PTT fluid around a confined square is considered in this study under the isothermal conditions. The flow system is sketched as in Figure 1. The blockage ratio is 1/4. The continuity, momentum and constitutive PTT equations in rectangular coordinates  $(x, y)$  are presented in Equations (1) and (2). For a two-dimensional flow system equation can be given as:

Continuity

$$\frac{\partial u}{\partial x} + \frac{\partial v}{\partial y} = 0$$

x-momentum

$$\frac{\partial}{\partial x} \left( Re uu - (1 - w_r) \frac{\partial u}{\partial x} \right) + \frac{\partial}{\partial y} \left( Re vu - (1 - w_r) \frac{\partial u}{\partial y} \right) = - \frac{\partial p}{\partial x} + \frac{\partial \tau_{xx}}{\partial x} + \frac{\partial \tau_{xy}}{\partial y} \tag{1}$$

y-momentum

$$\frac{\partial}{\partial x} \left( Re uv - (1 - w_r) \frac{\partial v}{\partial x} \right) + \frac{\partial}{\partial y} \left( Re vv - (1 - w_r) \frac{\partial v}{\partial y} \right) = - \frac{\partial p}{\partial y} + \frac{\partial \tau_{xy}}{\partial x} + \frac{\partial \tau_{yy}}{\partial y}$$

Eq. (2) gives viscoelastic constitutive linear PTT mode.1.<sup>10</sup> This viscoelastic model serves shear thinning and normal stress effects in the flow field. Dimensionless forms of the stress components  $\tau_{xx}$ ,  $\tau_{yy}$ ,  $\tau_{xy}$  are given as follows:

### Phan-Thien-Tanner (PTT) constitutive equation:

Stress components of  $\tau_{xx}$

$$\left( 1 + \varepsilon \frac{We}{w_r} (\tau_{xx} + \tau_{yy}) \right) \tau_{xx} + \frac{\partial}{\partial x} (We u \tau_{xx}) + \frac{\partial}{\partial y} (We v \tau_{xx}) = We \left( \frac{\partial u}{\partial y} - \frac{\partial v}{\partial x} \right) \tau_{xy} + 2We \frac{\partial u}{\partial x} \tau_{xx} + We \left( \frac{\partial u}{\partial y} + \frac{\partial v}{\partial x} \right) \tau_{xy} + 2w_r \frac{\partial u}{\partial x} \tag{2}$$

Stress components of  $\tau_{yy}$

$$\left( 1 + \varepsilon \frac{We}{w_r} (\tau_{xx} + \tau_{yy}) \right) \tau_{yy} + \frac{\partial}{\partial x} (We u \tau_{yy}) + \frac{\partial}{\partial y} (We v \tau_{yy}) = We \left( \frac{\partial v}{\partial x} - \frac{\partial u}{\partial y} \right) \tau_{xy} + 2We \frac{\partial v}{\partial y} \tau_{yy} + We \left( \frac{\partial u}{\partial y} + \frac{\partial v}{\partial x} \right) \tau_{xy} + 2w_r \frac{\partial v}{\partial y}$$

Stress components of  $\tau_{xy}$

$$\left( 1 + \varepsilon \frac{We}{w_r} (\tau_{xx} + \tau_{yy}) \right) \tau_{xy} + \frac{\partial}{\partial x} (We u \tau_{xy}) + \frac{\partial}{\partial y} (We v \tau_{xy}) = - \frac{1}{2} We (\tau_{xx} - \tau_{yy}) \left( \frac{\partial u}{\partial y} - \frac{\partial v}{\partial x} \right) + w_r \left( \frac{\partial u}{\partial y} + \frac{\partial v}{\partial x} \right) + \frac{1}{2} We (\tau_{xx} + \tau_{yy}) \left( \frac{\partial u}{\partial y} + \frac{\partial v}{\partial x} \right)$$

where  $u, v$  are the velocities,  $p$  is the pressure,  $w_r = 1 - \beta$  and the parameter  $\beta$  is the ratio of the retardation and relaxation time and  $\varepsilon$  is extensibility parameter. The Reynolds number ( $Re$ ) and the Weissenberg number ( $We$ ) which is defined as the ratio of characteristic fluid relaxation time to characteristic time scale in the flow are given through ( $Re = \rho UH / \eta_0$ ), where  $\eta_0$  is the total viscosity of polymer and solvent, and  $We = \lambda u / H$ , where  $\lambda$  is relaxation constant of the viscoelastic fluid.  $Re$  is important dimensionless number to characterize flow pattern and it compares the inertial and viscous forces in the flow field.  $We$  is the other dimensionless number that describes the dominance of elastic forces over viscous forces of the flow. The material parameters  $\beta$  and  $\varepsilon$  are set as 0.2 and 0.25, respectively.

A finite volume method<sup>11,12</sup> is used to obtain discrete form of the flow equations. Convective terms in the PTT equations are computed by using of CUBISTA<sup>13</sup> scheme. The detailed numerical methods have been also presented in the study of Tezel and co-workers.<sup>14</sup>

### 3. RESULTS AND DISCUSSION

Nonhomogeneous structured mesh is employed to simulate the flow field with  $B = 1/4$ . Smallest mesh size is used near the obstacle walls in order to resolve thin boundary layers and high gradients in the flow as depicted in Figure 1. Minimum size of the mesh has  $\Delta_x = 0.02$  and  $\Delta_y = 0.01$ . Total number of the cells is 372 x 162.

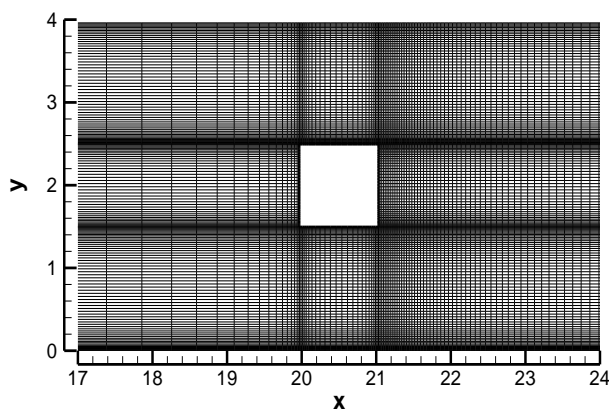


Figure 1. Non-uniform mesh structure around the square obstacle.

Viscoelastic fluids have normal stresses ( $\tau_{xx}$ ) due to revealing the elastic effects of the fluid flow rather than Newtonian flow. Normal stresses are resulted from velocity ( $ux$ ) changings through the flow direction. Figures 2a and 2b depict the impact of the  $We$  numbers on the normal stress component  $\tau_{xx}$  at creeping flow. In these figures dimensionless stress values are -0.1 and 1.

Symmetric normal stress field is observed. In the flow direction, normal stresses go further at the top and bottom of the obstacle. As  $We$  is increased, normal stress contours stretch longer distances in the behind of the obstacle (wake region). Otherwise, at the channel wall there is no amending normal stress profile with respect to  $We$ . When  $We$  is 15, the impact of elasticity seems to be by the extent of the shear thinning compared to the case of  $We = 5$ . As in Figure 2b negative normal stresses occur around the obstacle. These stresses dominantly develop in front of the object. When at  $We = 15$ , there is no observation of a negative normal stress as in Figure 2b due to high elasticity of the flow. At the front of the obstacle, sudden separated flows near the front of the obstacle cause the formation of Hoop stresses. It can be explained as larger normal stress changings through the tangential direction in the flow field due to stretching of elastic forces over the surface of the square cylinder. Similar findings are also offered for the circular cylinder by Oliveira and co-workers.<sup>13</sup> This formation of Hoop stresses comes from the sudden velocity changings in front surface of the square cylinder.

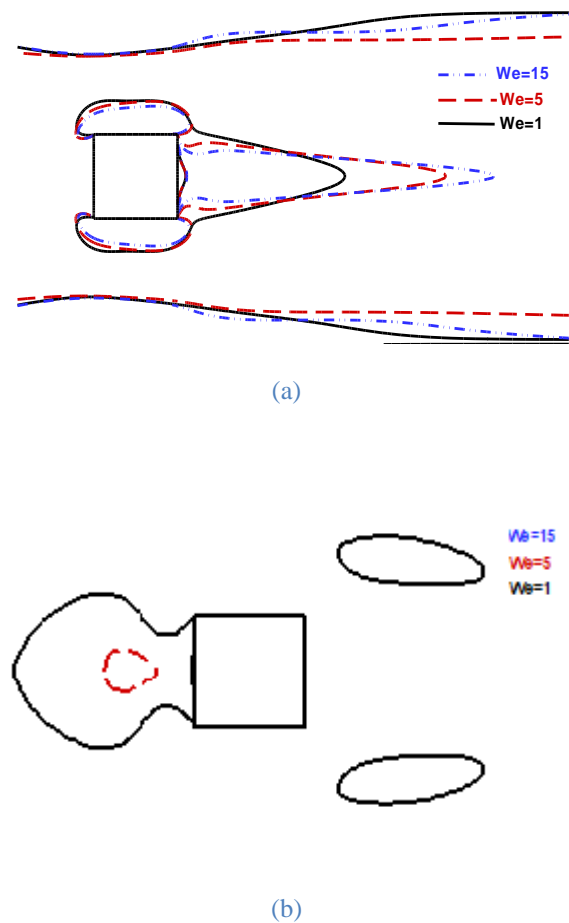
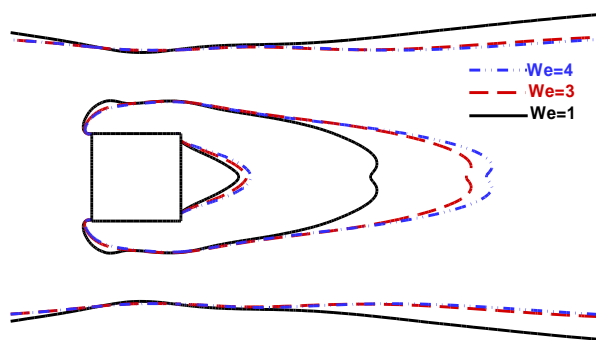
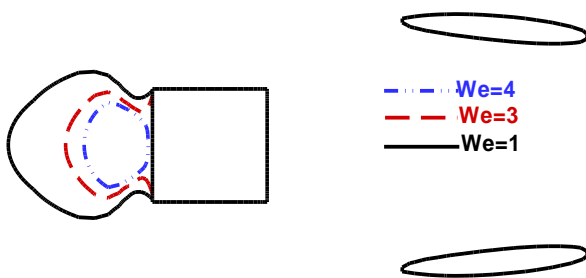


Figure 2. Normal stress profile for  $Re = 0$  at contour values a) 1 b) -0.1.

Figures 3 and 4 depict the normal stress field at  $Re = 10$  and  $Re = 20$ , respectively. Due to the stability problems encountered in the numeric solutions,  $We$  was capped at 4. As increased  $Re$ , behind the obstacle (in the wake region), normal stress field grows up to bigger size. As shown in Figure 4a, at  $Re = 20$ , normal stress divides into two symmetric fields in the wake region. Negative stress fields occur in this region since dominance of Hoop stresses. Due to the  $We$  ranges in Figures 3b and 4b, an increase in the extent of the stress fields is observed near the channel wall suggesting weaker shear thinning effects than  $We = 15$  case in Figure 2b. With the higher values of  $We$ , normal stresses modify progressively around the cylinder reported as in Norouzi and co-workers's study.<sup>15</sup>

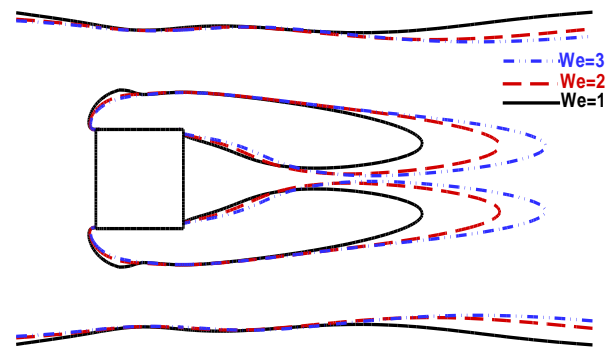


(a)

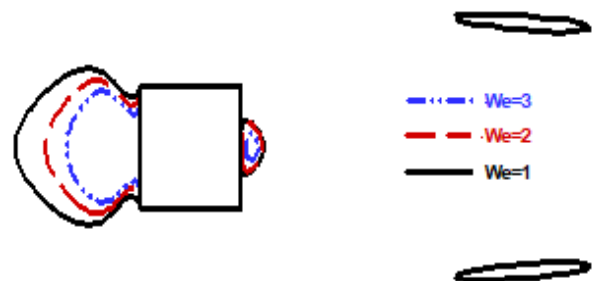


(b)

Figure 3. Normal stress profile for  $Re = 10$  at the contour value a) 1, b) -0.1.



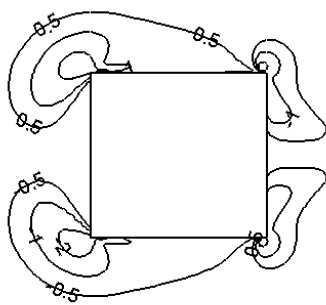
(a)



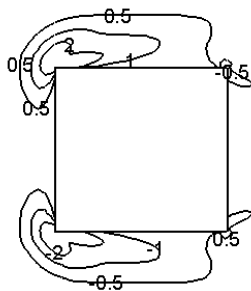
(b)

Figure 4. Normal stress profiles for  $Re = 20$  at the contour value a) 1, b) -0.1.

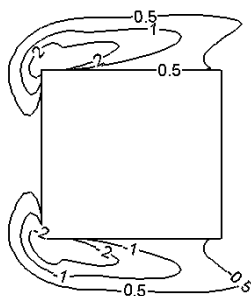
Figure 5 shows the effect of the  $Re$  on the shear stress field,  $\tau_{xy}$ . Shear stress is caused by viscous forces between the fluid molecules. Hence,  $u_x$  changes with respect to the perpendicular direction to the flow field. At the front corners of obstacle, hoop stresses cause the higher shear stress distribution due to instantaneous variation in viscoelastic flow velocity. At creeping flow, as shown in Figure 5a, at the back corners of the obstacle shear stresses also occur. As  $Re$  increases, at the front corners' higher values of the shear stress distend to the upper and lower surfaces of the obstacle as in Figure 5b and 5c due to flow separation effect of viscoelastic flow especially in the front corners.



(a)



(b)



(c)

**Figure 5.** Shear stress profile for  $We = 3$ , a)  $Re = 0$ , b)  $Re = 10$ , c)  $Re = 20$ .

#### 4. CONCLUSIONS

In the present study, normal and shear stresses distribution of viscoelastic fluid flowing over the obstacle is studied using numerical method. The results of the study can be summarized as follows.

- For stable solutions, at higher value of  $Re$  there is the lowest limit of  $We$  and at lower value of  $Re$  there is highest limit of  $We$ .
- Low  $We$  and high  $Re$  conditions supply the occurrence of negative normal stresses in the flow field.

- When the fluid inertia increases, in the wake region normal stresses get bigger size and the stress region is observed at the top and bottom surfaces of the pipe.
- Shear stresses occur in the flow region when the fluid flow is tangential to the boundaries of the obstacle at increased  $Re$

#### Conflict of interests

Authors declare that there is no a conflict of interest with any person, institute, company, etc.

#### REFERENCES

1. Liang, C.; Papadakis, G.; Luo, X. *Comput. Fluids* **2009**, 38, 950-964.
2. Hassanzadeh, R.; Sahin, B.; Ozgoren, M. *Int. J. Comput. Fluid D.* **2011**, 25, 535-545.
3. Breuer M.; Bernsdorf, M.; Zeiser, T.; Durst, T. *Int. J. Heat Fluid Fl.* **2000**, 21, 186-196.
4. Sen, S.; Mittal, S.; Biswas, G. *Int. J. Numer. Meth. Fl.* **2011**, 67, 1160-1174.
5. Puig-Aranega, A.; Burgos, J.; Cito, S.; Cuesta, I.; Saluena, C. *Int. J. Comput. Fluid D.* **2015**, 29, 434-446.
6. Dhiman, A.K.; Chhabra, R.P.; Eswaran, V. *J. Non-Newton. Fluid Mech.* **2008**, 148, 141-150.
7. Dhiman, A.K.; Chhabra, R.P.; Eswaran, V. *J. Chem. Eng. Res. Des.* **2006**, 84, 300-310.
8. Ehsan, I.; Mohammad, S.; Reza, N.; Ali, J. *Int. J. Phys. Sci.* **2012**, 7, 988-1000.
9. Nirmalkar, N., Chhabra R.P.; Poole R.J. *J. Non-Newton. Fluid Mech.* **2012**, 171-172, 17-30.
10. Phan-Thien, N.; Tanner, R.I. *J. Non-Newton. Fluid Mech.* **1977**, 2, 353-365.
11. Patankar, S.V.; Spalding, D.B. *Int. J. Heat Mass Tran.* **1972**, 15, 1787.
12. Versteeg H. K.; Malalasekera W. An introduction to computational fluid dynamics: The finite volume method, 2nd Edition, Prentice Hall, USA, 1995.
13. Alves, M.A., Oliveira P.J.; Pinho F.T. *Int. J. Numer. Meth. Fl.* **2003**, 4, 47-75.


**DOI:** <http://dx.doi.org/10.32571/ijct.549930>


**E-ISSN:**2602-277X


14. Tezel, G. B.; Yapici, K.; Uludag, Y. *Period Polytech. Chem. Eng.* **2019**, 63, 190-199.

15. Norouzi, M.; Varedi, S.R.; Zamani, M. *Korea-Aust. Rheol. J.* **2015**, 27, 213-225.

## ORCID

 <https://orcid.org/0000-0002-0671-208X> (G.B. Tezel)

 <https://orcid.org/0000-0002-3902-9375> (K. Yapici)

 <https://orcid.org/0000-0002-2151-5818> (Y. Uludag)